Catalysis Today 267 (2016) 167–176

Contents lists available at ScienceDirect

Catalysis Today

journal homepage: www.elsevier.com/locate/cattod

# Spectroscopic investigation of sulfur-resistant $Pt/K_2O/ZrO_2/TiO_2/Al_2O_3$ NSR/LNT catalysts

Z. Say, M. Tohumeken, E. Ozensoy*

*Department of Chemistry, Bilkent University, 06800 Ankara, Turkey*

ARTICLE INFO

*Article history:*
Received 6 October 2015
Received in revised form
25 November 2015
Accepted 4 December 2015
Available online 18 January 2016

*Keywords:*
NSR/LNT
$DeNO_x$ $Al_2O_3/ZrO_2/TiO_2$
FTIR
TPD

ABSTRACT

An alternative ternary support oxide material and its $K_2O$ and Pt functionalized counterparts in the form of $Pt/K_2O/Al_2O_3/ZrO_2/TiO_2$ with different $K_2O$ loadings were synthesized. Structural and morphological properties of the catalysts were characterized *via* XRD and BET techniques in comparison to a conventional Pt/20Ba/Al benchmark NSR/LNT catalyst. Comprehensive *in-situ* FTIR and TPD analysis revealed that increasing the $K_2O$ loading in the $Pt/K_2O/AZT$ system leads to an increase in $NO_x$ Storage Capacity (NSC) at the expense of the formation of bulk-like sulfates requiring higher temperature for complete sulfur elimination with $H_2$(g). Observed delicate trade-off between NSC and sulfur poisoning tendencies of the currently investigated family of AZT-based NSR/LNT catalysts implies that $Pt/5.4K_2O/AZT$ is a promising catalyst revealing comparable NSC within the temperature range of 473–673 K to that of the conventional Pt/20Ba/Al benchmark catalyst, while exhibiting superior sulfur tolerance and regeneration characteristics.



## 1. Introduction

$NO_x$ emitted from mobile sources have serious destructive effects on the atmosphere, global ecosystem and especially on the human health. About one half of the total $NO_x$ emissions results from mobile sources [1]. While the very first regulations for diesel engine emissionswere primarily focusing on particle emissions, other hazardous pollutants such as CO, $SO_2$, $NO_x$ and unburned hydrocarbons from mobile sources are currently being regulated with increasingly stringent limitations. This leads to a constant pressure on the global automotive industry to develop novel and innovative aftertreatment technologies that can satisfy the continuously evolving environmental legislations and to lower the exhaust emission levels [2–4]. Recently, it was reported that $NO_x$ emissions of some of the currently existing diesel-engine passenger cars equipped with modern $DeNO_x$ aftertreatment systems on the highway were up to 20–35 times higher than that of the allowed emission limits [5]. Furthermore, a very recent study published by the European Environment Agency (EEA) [6] reported that without any exception, each European Union (EU) member state violates at least one or more of the existing annual emission limitations associated with $NO_x$, $SO_x$, $NH_3$ and non-methane volatile organic compounds (NMVOC). Among these EU member states, particularly Germany, Austria and Ireland were found to fail meeting annual European $NO_x$ emission standards in 2014. These striking examples clearly call for the design and development of more efficient, more stable and more affordable heterogeneous catalytic architectures that can be used in modern $DeNO_x$ aftertreatment technologies.

For lean-burn engines, a promising aftertreatment method for the catalytic $NO_x$ reduction is the so called $NO_x$ storage/reduction (NSR)/Lean $NO_x$ Trap (LNT) technology [7,8]. A typical NSR/LNT catalyst is comprised of basic oxides (*e.g.* BaO, $K_2O$), redox sites (*e.g.* Pt, Pd and/or Rh) and a high surface area support material (*e.g.* $\gamma$-$Al_2O_3$) [2,3,9].

The conventional NSR/LNT catalyst, $Pt/BaO/\gamma$-$Al_2O_3$, exhibits efficient $NO_x$ conversion and storage performance within the operational temperature window of the diesel emission tail pipe (*i.e.* 473–673 K) [10–18]. However, recent engine applications such as the fuel-efficient gasoline direct injection (GDI) engines require catalytic aftertreatment solutions which should be able to operate at temperatures above 400 °C, where the conventional NSR/LNT catalysts cannot function effectively [19]. Toyota Motor Company

* Corresponding author.
*E-mail address:* ozensoy@fen.bilkent.edu.tr (E. Ozensoy).

http://dx.doi.org/10.1016/j.cattod.2015.12.013
0920-5861/

reported that $K_2O$ and BaO are two of the most promising $NO_x$ storage components to be used in NSR/LNT catalysts [20]. Among these two different types of basic metal oxides, the use of $K_2O$ attracted particular interest due to its superior $NO_x$ storage capacity (NSC) at elevated temperatures [21]. Other noteworthy advantages of $K_2O$ domains are associated to their stronger basicity and the lack of unfavorable solid-state interactions between $K_2O$ and the $\gamma$-$Al_2O_3$ support material, unlike that of BaO which may lead to the formation of undesired $BaAl_2O_4$ at high temperatures [22]. Luo et al. investigated the effect of $K_2O$ loading (within 2–20 wt. %) on the NSC of the $Pt/K_2O/\gamma$-$Al_2O_3$ system. It was found out that the catalyst formulation containing 10 wt. % $K_2O$ resulted in the highest NSC values within a wide temperature window of 523–823 K [22].

In addition to the promising NSC of $K_2O$-functionalized materials in high temperature $DeNO_x$ applications, sulfur-poisoning tolerances as well as the sulfur regeneration characteristics of such systems should be also taken into consideration. It is known that $K_2O$ domains dispersed on a $\gamma$-$Al_2O_3$ support material are highly prone to sulfur poisoning, experiencing rapid and rather irreversible catalytic deactivation. A class of novel Al/Ti/Zr mixed oxides has emerged in recent years with enhanced surface and structural properties as support for $K_2O$-based NSR/LNT catalysts [23–25]. In recent studies, $ZrO_2/TiO_2$, $TiO_2/Al_2O_3$ and $Al_2O_3/ZrO_2/TiO_2$-supported NSR/LNT catalysts can reveal superior sulfur regeneration and $NO_x$ recovery performances as compared to that of $\gamma$-$Al_2O_3$-based systems (*i.e.* $Pt/BaO/Al_2O_3$ *vs.* $Pt/K_2O/Al_2O_3$) [26,27]. Takashi et al. reported that a $ZrO_2$:$TiO_2$ support material with a mass ratio of 70:30 (which also revealed the highest SSA among the investigated materials therein) exhibited the best performance in terms of sulfur resistance, thermal durability and $NO_x$ abatement [28]. Their studies which also included Pt/Rh/Ba/K/AZT catalyst with nano-composite ternary oxide $Al_2O_3/ZrO_2/TiO_2$-support showed excellent $NO_x$ storage capacity (NSC) compared to that of $\gamma$-$Al_2O_3/ZrO_2/TiO_2$-support, where $\gamma$-$Al_2O_3$ was physically mixed with $ZrO_2/TiO_2$ [29,30]. In addition, Zou et al. [27] performed a detailed analysis on the effect of $Al_2O_3$ doping into the $ZrO_2/TiO_2$ matrix, suggesting that the Al:(Ti + Zr) atomic ratio of 3:1 exhibited the highest NSC for fresh and sulfur-regenerated catalyst. In a more recent work, Zou et al. studied the effect of K loading on the NSC and sulfur regeneration performance of $Pt/K/Al_2O_3/ZrO_2/TiO_2$ catalyst under realistic flow conditions [31].

However, these aforementioned comprehensive studies included a limited number of spectroscopic investigations on the interactions between $SO_x$ species and the corresponding catalyst surfaces. Thus, in the current work, we focus on the molecular level investigation of the fundamental interactions that take place between $SO_x$ species and K-based novel NSR/LNT catalyst surfaces in a qualitative and a semi-quantitative manner. Along these lines, we investigate the $SO_x$ adsorption/uptake as well as the $SO_x$ reduction/regeneration/release properties of $Al_2O_3/ZrO_2/TiO_2$ (AZT) supported Pt/K/AZT catalysts in comparison to a benchmark NSR/LNT catalyst (*i.e.* $Pt/BaO/Al_2O_3$) by utilizing *in-situ* spectroscopic techniques. Generation of S-containing surface functional groups, their thermal evolution, reduction and releases a function of temperature and $K_2O$ loading are systematically monitored by means of *in-situ* Fourier Transform Infrared Spectroscopy (*in-situ* FTIR) and Temperature Programmed Desorption (TPD). Moreover, structural and morphological properties of the synthesized materials are also analyzed *via* X-ray Diffraction (XRD) and Brunauer, Emmett and Teller (BET) surface area analysis techniques. Current results provide valuable molecular level insight regarding the interaction of $SO_x$ species with K-based NSR/LNT catalysts supported on novel AZT mixed oxide surfaces and the delicate trade-off between the NSC and sulfur poisoning phenomena.

## 2. Experimental

### 2.1. Material synthesis

#### 2.1.1. Synthesis of $Pt/Al_2O_3/ZrO_2/TiO_2$

$Al_2O_3/ZrO_2/TiO_2$ (AZT) support material was synthesized as described in one of our former publications where the relative composition of the ternary oxide system (*i.e.* $Al_2O_3/ZrO_2/TiO_2$) by mass was 50:35:15 [25]. 1 wt. % platinum-incorporated ternary oxide materials were synthesized by incipient wetness impregnation method using a solution of $Pt(NH_3)_2(NO_2)_2$ (Aldrich, diamminedinitritoplatinum(II), 3.4 wt.% solution in dilute $NH_3$(aq)). Prior to the Pt addition, $Al_2O_3/ZrO_2/TiO_2$ was initially calcined in air at 973 K for 150 min in order to remove the organic functionalities in the precursor. After the Pt-incorporation, Pt/AZT material was subsequently calcined in air at 973 K for 150 min in order to remove nitrite/nitrate originating from the Pt precursor and to structurally stabilize the catalyst surface.

#### 2.1.2. Synthesis of $Pt/K_2O/Al_2O_3/ZrO_2/TiO_2$

$K_2O$-based catalysts were also prepared *via* wetness impregnation. $Pt/K_2O/Al_2O_3/ZrO_2/TiO_2$ catalysts with 2.7, 5.4 and 10.0 wt. % $K_2O$ loading (*i.e.* $Pt/2.7K_2O/Al_2O_3/ZrO_2/TiO_2$, $Pt/5.4K_2O/Al_2O_3/ZrO_2/TiO_2$ and $Pt/10K_2O/Al_2O_3/ZrO_2/TiO_2$; respectively) were prepared *via* impregnation of $Al_2O_3/ZrO_2/TiO_2$ support (initially calcined at 973 K for 150 min) with an aqueous solution of potassium nitrate ($KNO_3{\cdot}6H_2O$, >99.0 %, Fluka, France) followed by calcination at 873 K for 150 min in order to thermally remove the nitrate content present in the precursors. Finally, $K_2O/Al_2O_3/ZrO_2/TiO_2$ structure was impregnated with the $Pt(NH_3)_2(NO_2)_2$ precursor and calcined at 973 K for 150 min under ambient conditions in order to attain 1 wt. % nominal precious metal loading. Throughout the current text, synthesized $Pt/K_2O/Al_2O_3/ZrO_2/TiO_2$ catalysts with 2.7, 5.4 and 10.0 wt. % $K_2O$ and 1 wt. % Pt loadings will be abbreviated as Pt/2.7K/AZT, Pt/5.4K/AZT and Pt/10K/AZT, respectively.

#### 2.1.3. Synthesis of $Pt/BaO/\gamma$-$Al_2O_3$

For the synthesis of the Pt/20BaO/Al benchmark catalyst, $\gamma$-$Al_2O_3$ support material (SASOL Puralox, 210 $m^2/g$) was impregnated with an aqueous solution of barium nitrate ($Ba(NO_3)_2$, ACS Reagent, $\geq$ 99%, Riedel-de Häen, Germany) which was followed by calcination at 873 K in air for 150 min. Finally, $20BaO/Al_2O_3$ was impregnated with the $Pt(NH_3)_2(NO_2)_2$ precursor (Aldrich, diamminedinitritoplatinum(II), 3.4 wt. % solution in dilute$NH_3$(aq)) to obtain 1 wt. % nominal precious metal loading, followed by calcination at 973 K for 150 min. This catalyst will be abbreviated as Pt/20Ba/Al throughout the current text.

### 2.2. Experimental setup

Comprehensive description of the custom-made batch-mode *in-situ* FTIR and TPD spectroscopic setup used in the current measurements can be found elsewhere [10,14,25,32]. Briefly, an FTIR spectrometer (Bruker Tensor 27) and a quadruple mass spectrometer (QMS, Stanford Research Systems, RGA 200) were simultaneously connected to a batch-type spectroscopic reactor. FTIR experiments were performed in transmission mode. TPD profiles were obtained under vacuum by using a computer-controlled linear temperature ramp of 12 K/min with a maximum sample temperature of 1173 K.

### 2.3. Experimental procedures

#### 2.3.1. Monitoring $SO_x$ adsorption via in-situ FTIR

Sulfur adsorption/poisoning characteristics of each material was investigated by exposing the catalyst surfaces to a 2.0 Torr $SO_2 + O_2$ gas mixture ($SO_2$:$O_2$ = 1:10, v/v) at 323 K ($SO_2$ purity >99%, Air Products; $O_2$ purity > 99.999%, Linde GmbH). After the introduction of $SO_x$ mixture at 323 K, samples were annealed to 373, 473, 573 and 673 K for 5 min in the presence of the $SO_x$ mixture. FTIR spectra of these sulfated surfaces were acquired after cooling to 323 K in the presence of the gas mixture and subsequent evacuation to < $10^{-3}$ Torr. It should be noted that the effective concentration of $SO_2$ used in the current poisoning experiments corresponds to *ca.* 263 ppm (in a balance carrier gas under flow conditions), which translates into extremely severe poisoning conditions considering the typical sulfur content (15 ppm) of Ultra Low Sulfur Diesel (ULSD) fuel. Thus, the current poisoning experiments can be assessed as accelerated and extreme sulfur poisoning experiments, where the novel K-AZT based catalysts were exposed to particularly challenging conditions, where they can demonstrate their ultimate sulfur-regeneration capabilities.

#### 2.3.2. Monitoring $SO_x$ desorption via in-situ FTIR

Prior to $SO_x$ desorption experiments, materials were sulfated as described above by collecting a series of *in-situ* FTIR spectra in the presence of the $SO_x$ mixture as a function of temperature until 673 K. After the saturation of the surfaces with sulfur at 673 K, the reactor was evacuated to a pressure of <$10^{-2}$ Torr, followed by the introduction of 15.0 Torr of $H_2$(g) ($H_2$ purity > 99.999%, Linde GmbH) at 323 K. Next, poisoned catalysts were annealed under hydrogen atmosphere at 473, 673, 773, 873 and 973 K for 5 min. *In-situ* FTIR spectra were obtained after each $H_2$ exposure and by cooling the sample to 323 K in the presence of $H_2$.

#### 2.3.3. $SO_x$ desorption via TPD

Before the $SO_x$-TPD experiments, material surfaces were initially exposed to a 2.0 Torr $SO_2 + O_2$ gas mixture ($SO_2$:$O_2$ = 1:10) at 673 K for 30 min. Then the IR spectroscopic reactor was evacuated to a pressure lower than $10^{-3}$ Torr followed by heating under vacuum to 1173 K with a linear heating rate of 12 K/min. In the TPD experiments, $m/z$ = 32 (corresponding to $O_2$(g) desorption and S(g) formation due to the impact ionization-induced fragmentation of desorbed $SO_2$(g) species in QMS) and $m/z$ = 64 (corresponding to $SO_2$(g) desorption) channels were monitored *via* QMS.

## 3. Results and discussion

### 3.1. Material characterization

#### 3.1.1. X-ray diffraction analysis (XRD)

Fig. 1 illustrates the XRD patterns of Pt/AZT, Pt/2.7K/AZT, Pt/5.4K/AZT, Pt/10K/AZT and Pt/20Ba/Al. Apart from the presence of structurally well-ordered metallic platinum (JCPDS 001-1190), Pt/AZT and Pt/K/AZT catalysts given in Fig. 1 exhibit highly amorphous characteristics. On the other hand, material with 10.0 wt. % $K_2O$ (*i.e.* Pt/10.0K/AZT) reveals additional poorly discernible diffraction signals at $2\theta$ = 30.48°, 50.50°, 60.91° corresponding to tetragonal $ZrO_2$ (JCPDS 80-2155) together with some suppression of Pt diffraction features. XRD analysis of the benchmark Pt/20Ba/Al NSR/LNT catalyst reveals γ-$Al_2O_3$ (JCPDS 001-1303), $BaAl_2O_4$ (JCPDS 017-0306) and metallic Pt (JCPDS 001-1190) features. On the Pt/20Ba/Al catalyst, BaO domains interact with the γ-$Al_2O_3$ support at elevated temperatures yielding the formation of undesired $BaAl_2O_4$ phase as a result of thermal aging [2,3,33].

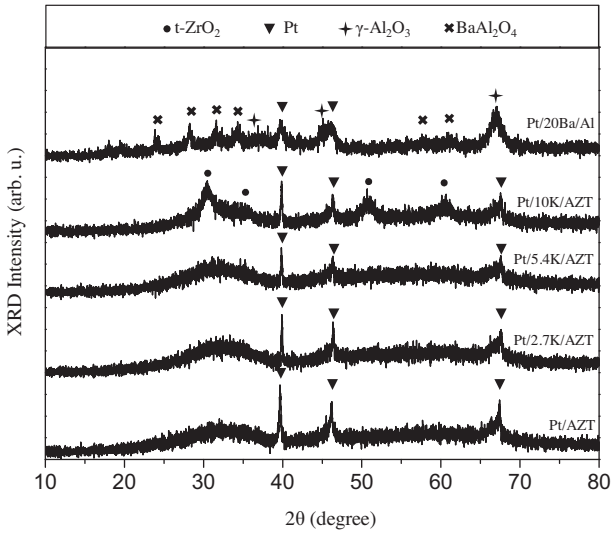


**Fig. 1.** XRD patterns corresponding to Pt/AZT, Pt/2.7K/AZT, Pt/5.4K/AZT, Pt/10K/AZT and Pt/20Ba/Al materials upon calcination at 973 K.

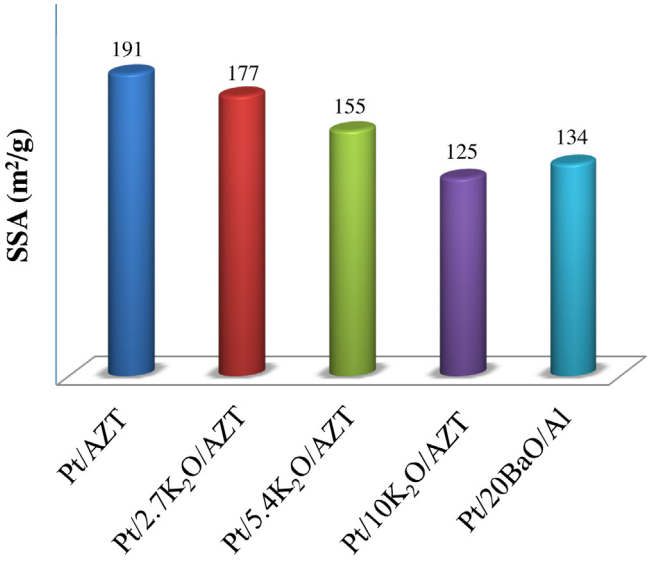


**Fig. 2.** BET specific surface area (SSA) values of the investigated materials.

#### 3.1.2. BET specific surface area (SSA) measurements

Fig. 2 illustrates SSA values for Pt/AZT, Pt/2.7K/AZT, Pt/5.4K/AZT, Pt/10K/AZT and Pt/20Ba/Al. SSA values for Pt/AZT is slightly higher than 2.7 wt. % $K_2O$-modified counterpart (*i.e.* Pt/2.7K/AZT). However, increase in the $K_2O$ loading from 2.7 wt. % to 5.4 and 10.0 wt. % monotonically decreases SSA values form 177 $m^2$/g to 155 and 125 $m^2$/g; respectively. It should be noted that the SSA value of the catalyst with the highest $K_2O$ loading was comparable to that of the benchmark Pt/20Ba/Al catalyst (134 $m^2$/g), while SSA values of all of the other catalysts were relatively higher.

### 3.2. $SO_x$ Uptake/adsorption via in-situ FTIR spectroscopy

Fig. 3 represents temperature-dependent adsorbed $SO_x$ species on Pt/AZT, Pt/2.7K/AZT, Pt/5.4K/AZT and Pt/10K/AZT material surfaces upon exposure to 2.0 Torr of $SO_2 + O_2$ gas mixture ($SO_2$:$O_2$ = 1:10). While the black-colored spectra in each panel correspond to the surface $SO_x$ species generated within a temperature range of 323–573 K, the topmost red spectra correspond to sulfur poisoning at 673 K.

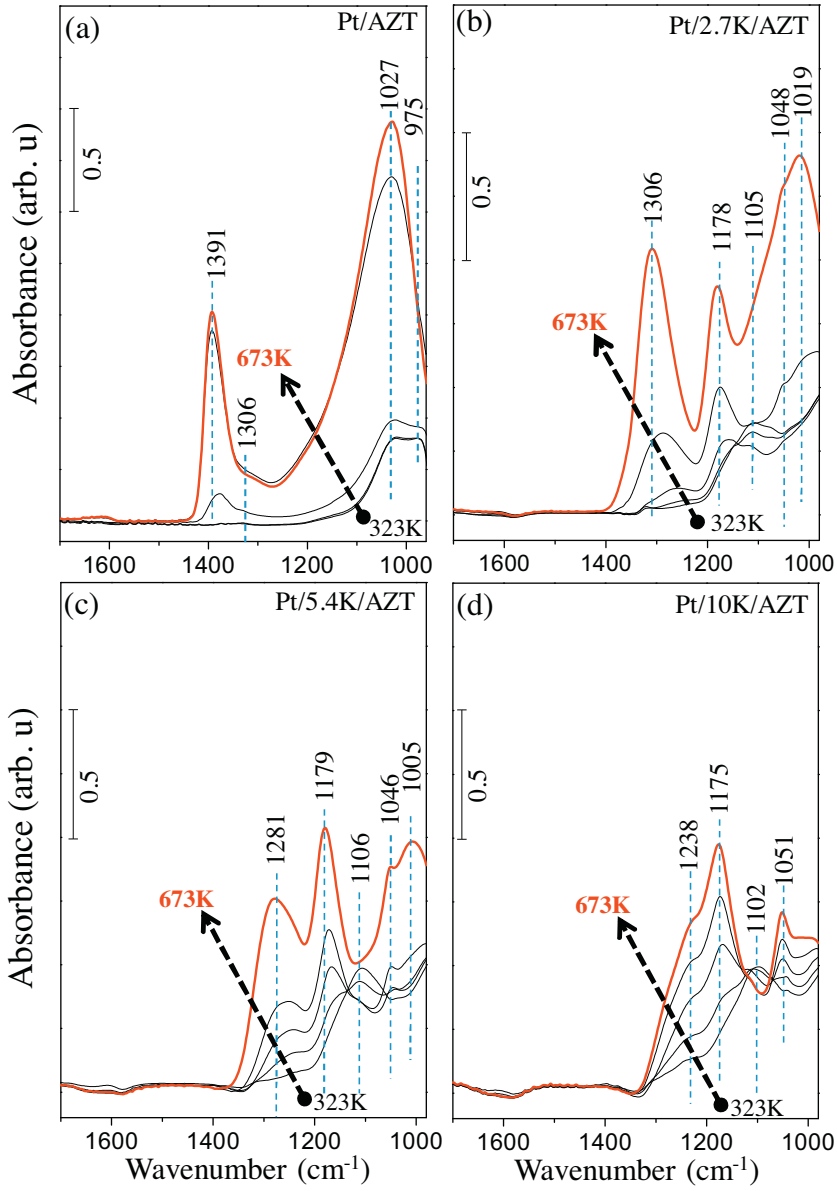


**Fig. 3.** FTIR spectra demonstrating the $SO_x$ uptake/adsorption properties of (a) Pt/AZT, (b) Pt/2.7K/AZT(c) Pt/5.4K/AZT and (d) Pt/10K/AZT surfaces. Black set of spectra in each panel were acquired after $SO_x$ exposure (2.0 Torr, $SO_2$:$O_2$ = 1:10) at 323 K, followed by annealing at 373, 473 and 573 K in the $SO_x$ gas mixture for 15 min and subsequent evacuation. Red spectra in each panel were recorded after $SO_x$ exposure at 673 K and subsequent evacuation. All spectra were recorded at 323 K in vacuum. (For the interpretation of the references to colour in this figure, the reader is referred to the web version of this article.)

Kim et al. reported that an increase in $K_2O$ loading from 2 wt. % to 30 wt. % led to a boost in NSC of $Pt/K_2O/Al_2O_3$ materials within 600–800 K [34]. As will be demonstrated latter, although such extremely high $K_2O$ loadings could be beneficial to enhance NSC in the absence of $SO_x$, they may also lead to irreversible sulfur poisoning in the presence of $SO_x$. Therefore, in the current study, we limited the $K_2O$ loading of the AZT-based NSR/LNT materials to 10 wt. %.

Fig. 3a shows that $SO_x$ adsorption on Pt/AZT at relatively lower temperatures (*i.e.* 323 and 373 K) leads to two main vibrational features located at 1027 and 975 $cm^{-1}$ which can be assigned to sulfate ($SO_4^{2-}$) and sulfite ($SO_3^{2-}$) functional groups, respectively [35–39]. Absorbance intensities of these two particular vibrational frequencies are comparable at low temperatures, while the sulfate feature starts to dominate the sulfite feature at higher temperatures. Thermally-triggered catalytic oxidation of sulfite species to sulfates on the Pt/AZT surface can also be followed in Fig. 3a by monitoring the growth of the antisymmetric stretching mode of surface sulfate groups located at 1391 and 1306 $cm^{-1}$ [14,40]. As illustrated in Fig. 3b–d, addition of basic $K_2O$ domains onto AZT ternary oxide system results in alteration of the spectral line shapes. Pt/2.7 K/AZT (Fig. 3b) presents five major vibrational features located at 1306, 1178, 1105, 1048 and 1019 $cm^{-1}$. While IR stretchings at 1306, 1105, 1048 and 1019 $cm^{-1}$ can be attributed to the surface sulfate ($SO_4^{2-}$) groups on $K_2O$ and/or on the AZT support, vibrational feature located at 1178 $cm^{-1}$ can be attributed to bulk-like sulfate groups on $K_2O$ [41,42]. This latter feature becomes more discernible with an increase in the $K_2O$ loading (*i.e.* 5.4 wt. % and 10 wt. %) evident by the increasing relative absorbance intensity of the 1178 $cm^{-1}$ signal in Fig. 3c and d. $SO_x$ adsorption on Pt/5.4K/AZT and Pt/10K/AZT materials at 673 K leads to vibrational features at 1281 and 1238 $cm^{-1}$ along with the absence of any significant vibrational bands located at *ca.* > 1300 $cm^{-1}$ (Fig. 3c and d). The vibrational signals at 1281 and 1238 $cm^{-1}$ can be assigned

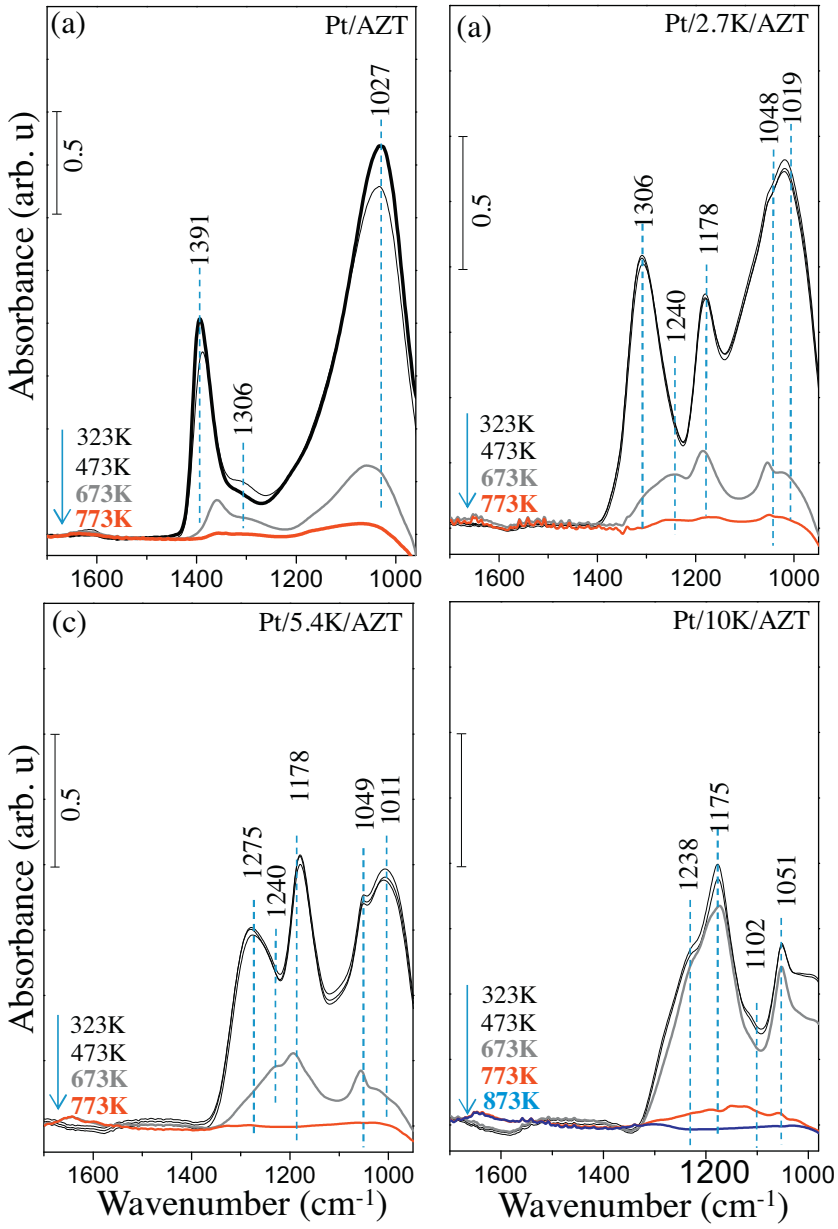


**Fig. 4.** FTIR spectra associated with $SO_x$ reduction and regeneration of (a) Pt/AZT, (b) Pt/2.7K/AZT(c) Pt/5.4K/AZT and (d) Pt/10K/AZT materials *via* $H_2$(g). Catalysts were initially sulfated (2.0 Torr, $SO_2$:$O_2$ = 1:10 for 15 min at 673 K) followed by evacuation and subsequent exposure to $H_2$(g) (15.0 Torr) at 323, 473, 673, 773, 873 and 973 K for 5 min. All spectra were recorded at 323 K.

to predominantly sulfates on $K_2O$ domains [14,41–43]. It can be argued that with the increasing $K_2O$ loading, an increasingly larger portion of the AZT surface is covered by $K_2O$ islands/domains, decreasing the extent of exposed/uncovered AZT surface. It is also likely that the increase in the $K_2O$ loading also results in the growth of the $K_2O$ particle size and formation of 3D agglomerates, enabling the storage of $SO_x$ in the form of bulk-like sulfates in the sub-surface of these 3D nanoparticles. This argument is also in good agreement with the measured SSA values presented in Fig. 2 suggesting that the increase in the $K_2O$ loading in the catalyst formulation leads to a monotonic decrease in the SSA as expected by sintering of the $K_2O$ domains and particle size growth.

### 3.3. *Sulfur regeneration with $H_2$(g)* via in-situ *FTIR spectroscopy*

As mentioned above, $SO_x$ reduction/regeneration performance has a significant influence on the catalyst lifetime and $NO_x$ storage capacity. Therefore, $SO_x$ reduction characteristics of synthesized materials were also studied as a function of temperature by means of *in-situ* FTIR spectroscopy. Fig. 4 illustrates the evolution of the S-containing surface functional groups on Pt/AZT, Pt/2.7K/AZT, Pt/5.4K/AZT and Pt/10K/AZT catalyst surfaces as a function of temperature within 323–773 K in the presence of an external reducing agent, $H_2$(g).

In these set of experiments, catalysts were initially saturated with a 2.0 Torr of $SO_2 + O_2$ gas mixture ($SO_2$:$O_2$ = 1:10) at 673 K for 5 min and then cooled to 323 K followed by the evacuation of the spectroscopic reactor, introduction of 15.0 Torr $H_2$(g) at 323 K and annealing in $H_2$(g) at the given temperatures within 323–773 K. This particularly chosen initial sulfation/poisoning temperature (*i.e.* 673 K) is not only relevant to realistic NSR/LNT operational temperatures, but is also high enough to activate $SO_2$ oxidation to sulfites and sulfates in a comprehensive manner. In the series of experiments given in Fig. 4, spectral line shapes do not typi-

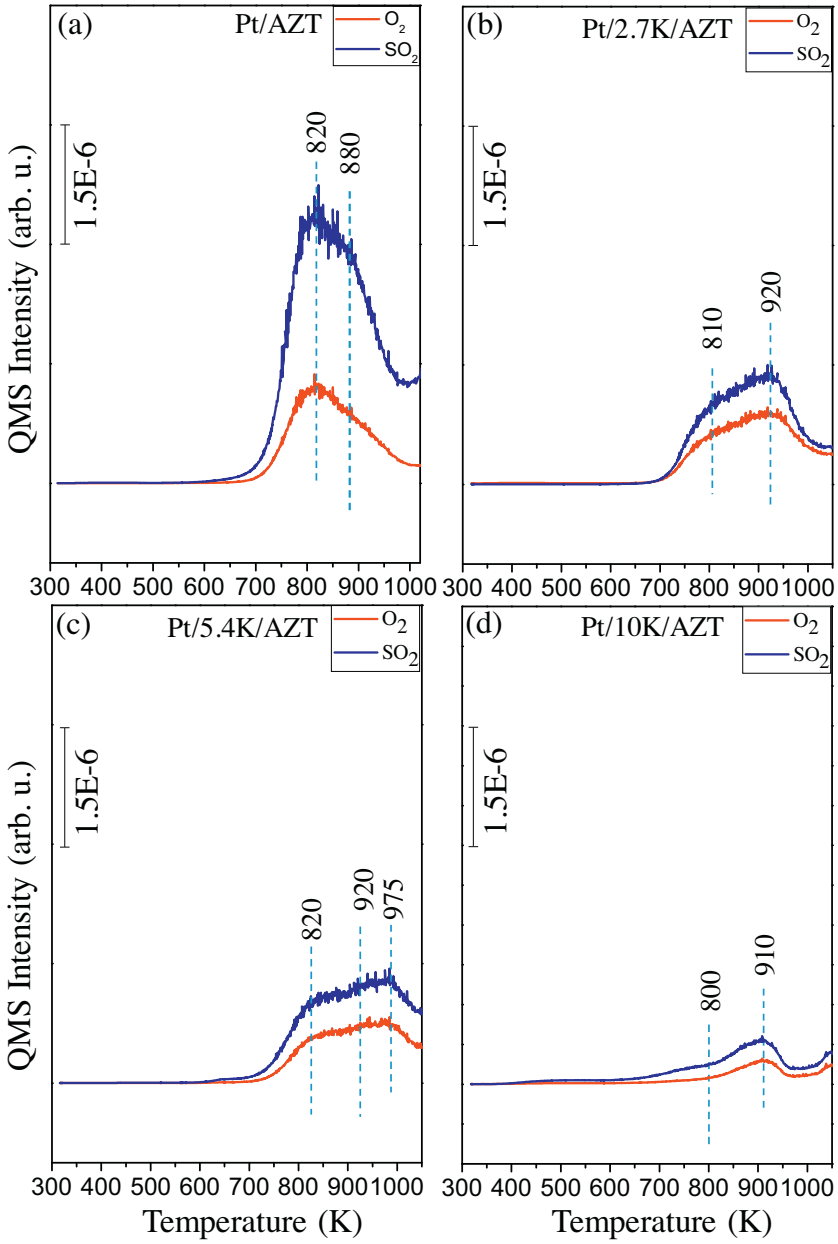


**Fig. 5.** TPD profiles for (a) Pt/AZT, (b) Pt/2.7K/AZT, (c) Pt/5.4K/AZT and (d) Pt/10K/AZT catalysts after 2.0 Torr $SO_x$ (2.0 Torr $SO_2 + O_2$, $SO_2:O_2 = 1:10$) adsorption at 673 K for 30 min and subsequent evacuation.

cally change in a noteworthy manner at reduction temperatures $\leq$ 473 K. However, increasing the reduction temperature to 673 K (gray spectra in Fig. 4a–c) leads to noticeable alterations in the FTIR spectra, where bulk and surface sulfate/sulfite species significantly attenuate for Pt/AZT, Pt/2.7K/AZT and Pt/5.4K/AZT. Increasing the temperature to 773 K in the presence of $H_2$ leads to the almost complete elimination of the $SO_x$-related vibrational signatures on Pt/AZT, Pt/2.7K/AZT and Pt/5.4K/AZT surfaces (red spectra in Fig. 4a–c). It can be seen in Supporting information Fig. 1 that when Pt/20Ba/Al benchmark NSR/LNT catalyst is exposed to an identical set of sulfation and subsequent reduction treatments, a significantly greater portion of sulfate/sulfite species continue to exist on the Pt/20Ba/Al catalyst even at 773 K in the presence of 15.0 Torr $H_2$(g). This comparative analysis clearly suggests that Pt/AZT, Pt/2.7K/AZT and Pt/5.4K/AZT catalysts exhibit a superior sulfur regeneration performance than that of the Pt/20Ba/Al catalyst, as this former set of materials can be fully de-sulfated at 773 K in the presence of $H_2$.

However, AZT-based catalysts with the highest $K_2O$ loading used in the current study (*i.e.* Pt/10K/AZT) not only showed unique sulfur uptake characteristics as presented in Fig. 3d which is dominated by bulk-like sulfates, but also revealed a fairly different $SO_x$-reduction profile in the presence of $H_2$ (Fig. 4d). As can be seen in Fig. 4, at relatively low temperatures (i.e. $T \leq 673$ K), a significant portion of the $SO_x$ species can already be eliminated from Pt/AZT, Pt/2.7K/AZT and Pt/5.4K/AZT surfaces. However, at $T \leq 673$ K, almost all of the S-related surface functional groups remain intact on Pt/10K/AZT. Even at a reduction temperature of 773 K, although Pt/AZT, Pt/2.7K/AZT surfaces can be fully regenerated (Fig. 4a–c), Pt/10K/AZT surface still remains partially blocked/poisoned by sulfur-containing functional groups and completely eliminated at only at $\geq$ 873 K (Fig. 4d).

### 3.4. *Sulfur regeneration under vacuum* via *TPD analysis*

TPD experiments were also carried out in vacuum in order to investigate the thermal regeneration ability of the synthesized catalysts after sulfur poisoning in the absence of a reducing agent, as well as to compare the relative adsorption strengths of $SO_x$ species residing on the poisoned catalyst surfaces. Prior to TPD experiments, each catalyst was exposed to 2.0 Torr $SO_2 + O_2$ gas mixture ($SO_2$:$O_2$ = 1:10) at 673 K for 30 min.

Fig. 5 shows the TPD spectra corresponding to the thermal decomposition of sulfates and sulfites on Pt/AZT, Pt/2.7K/AZT, Pt/5.4K/AZT and Pt/10K/AZT catalyst surfaces. In these TPD experiments, only $O_2$ and $SO_2$ desorption channels (corresponding to mass to charge ratios of $m/z$ = 32 and 64; respectively) revealed significant signals and other $SO_x$ or $H_2S$ species were not detectable. As in the case of the BaO-based conventional NSR/LNT catalyst (Supporting information Fig. 2), $SO_x$-related species adsorbed on Pt/AZT and its $K_2O$-incorporated counterparts reveal high thermal stability which is evident by the appearance of $SO_x$ desorption signals at $T$ > 700 K. Analysis of the general TPD line shapes given in Fig. 5a–c suggests that at least two different $SO_x$ desorption signals exist for Pt/AZT, Pt/2.7K/AZT and Pt/5.4K/AZT catalysts at T < 1050 K, revealing desorption maxima located at *ca.* 800–820 K and at 900–975 K. Furthermore, $SO_2$ desorption on these surfaces within 700–1050 K is accompanied by $O_2$ desorption, suggesting that sulfate/sulfite decomposition occurs in the form of simultaneous $SO_2 + O_2$ release. It should be noted that the contribution of the $SO_2$ gas to the $m/z$ = 32 signal due to electron-impact induced fragmentation of $SO_2$ in the QMS ionizer chamber is less than 10 %, suggesting that $m/z$ = 32 signal can be almost exclusively attributed to the evolution of $O_2$(g) from the catalyst surfaces.

It is visible in Fig. 5a–c that the TPD desorption maxima tend to shift towards higher temperatures with increasing $K_2O$ loading in the catalyst formulation. It can also be noticed that with increasing $K_2O$ loading to 5.4 wt. % (see Fig. 5c), relative intensity of the 820 K desorption feature which can be mostly associated with $SO_x$ species on AZT surface is suppressed, along with the generation of a high-temperature desorption shoulder at 975 K. This is in perfect agreement with the *in-situ* FTIR results presented in Fig. 3 suggesting that with increasing $K_2O$ surface coverage, extent of exposed (uncovered) AZT surface decreases along with an increase in the $K_2O$ particle size, facilitating the formation of bulk-like sulfates that are also thermally more stable than that of the sulfates on AZT.

It is also important to note that the $SO_x$ desorption is not complete in Fig. 5b–d even at 1050 K (*i.e.* the highest experimentally attainable temperature in the current TPD setup) as evident by the presence of a desorption tail at $T$ = 1050 K which is presumably extending well-beyond this temperature (as supported by the *in-situ* FTIR results that will be provided later in the text). This observation implies that while surface sulfates/sulfites present on AZT support and $K_2O$ domains fully decompose at temperatures below 920 K, bulk-like potassium sulfate species require higher desorption temperatures for complete thermal decomposition and desorption. In other words, presence of basic $K_2O$ domains yields strong binding sites for $SO_2$, leading to the formation of thermally stable surface and bulk-like $SO_x$ species.

On the other hand, a further increase in the $K_2O$ loading to 10 wt.% illustrates rather different $SO_x$ desorption characteristics (Fig. 5d). It is evident that the $SO_x$ desorption features at T < 1050 K are suppressed to a great extent, leading to a relatively minor desorption feature located at 910 K with a shoulder at *ca.* 810 K. Considering the significant $SO_x$ uptake of the Pt/10K/AZT catalyst surface demonstrated by the *in-situ* FTIR data given in Fig. 3d, it is clear that most of the sulfate/sulfite species on Pt/10K/AZT remain intact even after vacuum annealing up to 1050 K. This is also quantitatively presented in Fig. 6, which presents the integrated $SO_2$ TPD

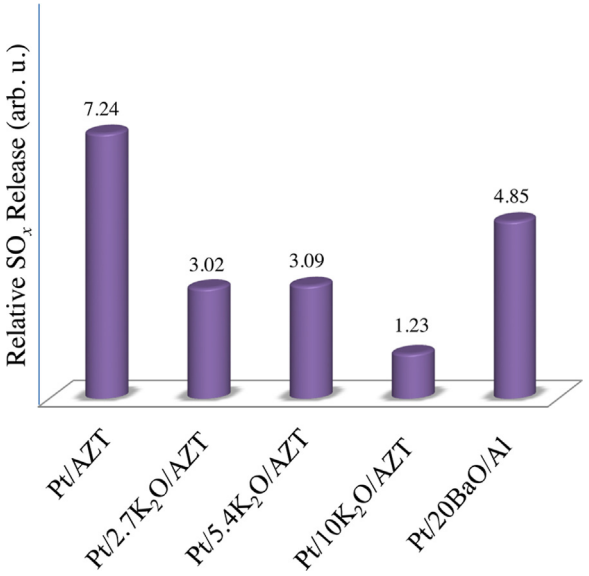


**Fig. 6.** Analysis of relative $SO_x$ release from investigated catalysts calculated *via* integrated TPD signals given in Fig. 5.

desorption signals for the investigated AZT-based catalysts within 323–1050 K. Fig. 6 illustrates that the integrated $SO_x$ desorption signal of Pt/AZT is roughly twice greater than that of Pt/2.7K/AZT and Pt/5.4K/AZT and also about four times greater than that of Pt/10K/AZT.

Figs. 3, 5 and 6, suggest that after the sulfation of the AZT-based catalysts at 673 K and a subsequent vacuum annealing up to 1050 K during the TPD experiments, a significant fraction of the sulfate and sulfite species remain intact on the K-containing sample surfaces. Thus, it is crucial to investigate the residual $SO_x$ species remaining on the K-containing AZT systems after the TPD runs. Fig. 7 shows such in-situ FTIR experiments corresponding to all of the investigated sulfur poisoned AZT-based catalysts before (black spectra) and after (red spectra) TPD experiments. Fig. 7a clearly indicates that in the absence of $K_2O$, sulfur-poisoned Pt/AZT catalyst can be almost fully regenerated *via* vacuum annealing up to 1050 K during the TPD experiments. On the other hand, Pt/2.7K/AZT catalyst which releases about % 50 lesser amount of $SO_x$ species during TPD (Fig. 6), still reveals a minor, yet readily detectable quantity of $SO_x$ (Fig. 7b). On the other hand, Pt/5.4K/AZT catalyst which has a comparable integrated $SO_x$ desorption signal to that of Pt/2.7K/AZT (Fig. 6), reveals a stronger residual $SO_x$ signal in the FTIR spectrum obtained after the TPD run given in Fig. 7c. This observation is in line with the fact that Pt/5.4K/AZT surface stores a significantly greater amount of $SO_x$ species (which are also thermally more stable) as compared to that of Pt/2.7K/AZT. Finally, residual sulfur analysis of the Pt/10K/AZT surface (Fig. 7d) indicates that almost all of the $SO_x$ species generated during initial poisoning process remain intact after the TPD run and vacuum annealing at 1050 K. Thus, it is apparent that the minor amount of $SO_x$ release during the TPD experiment for Pt/10K/AZT (Fig. 6) corresponds to a tiny fraction of the overall sulfur that is stored on this surface. This latter result has some resemblance to the TPD data corresponding to that of the Pt/20Ba/Al benchmark catalyst given in Supporting information Figs. 2 and 3 and also in Fig. 6 which also reveal an incomplete thermal regeneration upon vacuum annealing up to 1050 K during the TPD run.

We also performed a comprehensive investigation of the $NO_x$ storage, release and reduction characteristics of Pt/K/AZT systems *via in-situ* FTIR, TPD as well as quantitative flow-reactor experiments [44]. A detailed account of these additional experiments will

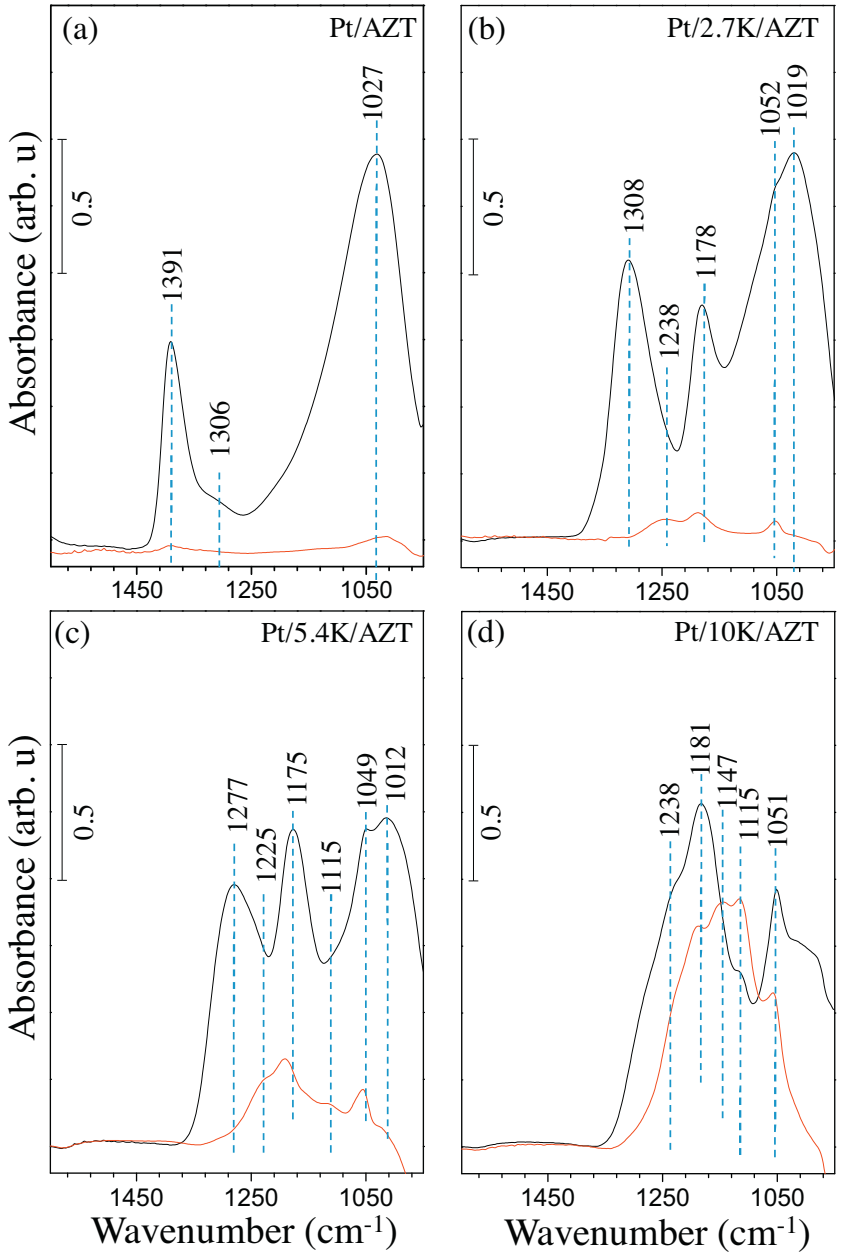


**Fig. 7.** FTIR spectra corresponding to $SO_x$ content of (a) Pt/AZT, (b) Pt/2.7K/AZT, (c) Pt/5.4K/AZT and (d) Pt/10K/AZT catalysts before (black) and after (red) $SO_x$-TPD runs. (For interpretation of the references to colour in this figure legend, the reader is referred to the web version of this article.)

be discussed thoroughly in a forthcoming report. Nevertheless, it is instructive to present relative integrated TPD $NO_x$ desorption signals obtained after saturation of the freshly prepared AZT-based catalysts with $NO_2$ (5.0 Torr $NO_2$ at 323 K for 10 min) in the absence of sulfur as compared to that of the Pt/20Ba/Al benchmark catalyst (Fig. 8). As can be seen in Fig. 8, relative $NO_x$ storage amounts of the AZT-based catalysts increase monotonically with increasing $K_2O$ loading until 5.4 wt. % $K_2O$, after which it converges to a value that is comparable to that of the Pt/20Ba/Al benchmark catalyst. It is worth mentioning that NSC of the synthesized materials were investigated in a flow-mode tubular reactor where the inlet gas feed was composed of 500 ppm NO, v.% 5 $O_2$, v.% 5 $CO_2$ and v.% 5 $H_2O$ balanced with Ar(g), revealing similar NSC values for Pt/5.4K/AZT (0.165 mmol/$g_{cat}$) and conventional Pt/20Ba/Al (0.171 mmol/$g_{cat}$) at 573 K [44].

A combined analysis of the structural characterization results as well as the spectroscopic probe molecule adsorption experiments given in the current study allows us to shed light on sulfur poisoning, regeneration and $NO_x$ storage characteristics of AZT-based NSR/LNT catalysts functionalized with $K_2O$. In the absence of the $K_2O$, Pt/AZT system reveals high SSA (191 $m^2/g$) and relatively weakly bound sulfates/sulfites which can readily be removed from the surface in a complete fashion either by reduction with $H_2$(g) at 773 K or simply by thermal regeneration in vacuum at *ca.* 950 K. However, due to lack of basic $K_2O$ domains, Pt/AZT suffers from relatively low NSC. Increasing the $K_2O$ loading to 2.7, 5.4 and 10.0 wt.% leads to a progressively increasing $NO_x$ adsorption where NSC seems to be converging to a value similar to that of Pt/20Ba/Al benchmark catalyst for Pt/5.4K/AZT and Pt/10K/AZT. Furthermore, Pt/5.4K/AZT sample allows complete removal of $SO_x$ *via* $H_2$(g) at 773 K unlike the conventional Pt/20Ba/Al benchmark

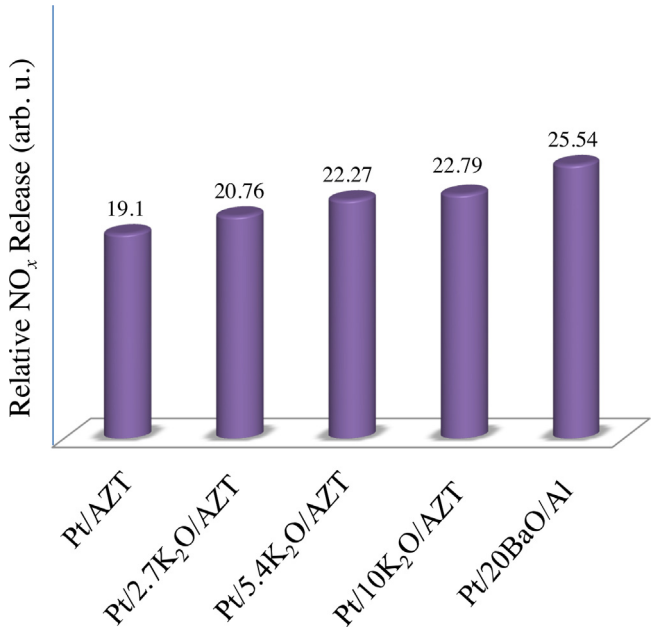


**Fig. 8.** Relative integrated $NO_x$ desorption signals obtained from $NO_x$-TPD experiments.

catalyst whose complete regeneration requires much higher temperatures (*i.e.* 973 K) under identical reducing conditions. Although increasing the $K_2O$ loading from 5.4 to 10.0 wt. % does not seem to have a tremendous enhancement in $NO_x$ adsorption properties of the Pt/K/AZT system, it does result in unfavorable $SO_x$ uptake, release and regeneration characteristics. TPD and FTIR data suggest that $K_2O$ domains tend to agglomerate with increasing $K_2O$ loading and form 3D clusters with growing $K_2O$ particle sizes. These phenomena also expedite the formation of bulk-like sulfate functionalities in the subsurface of $K_2O$ domains with much higher thermal stability and much stronger resistance against thermal decomposition and reduction with hydrogen. Consequently, Pt/5.4K/AZT system appears as a promising alternative which can also be used in conjunction with conventional Pt/20Ba/Al NSR/LNT catalysts.

## 4. Conclusion

In the current study, advanced ternary and quaternary mixed oxide materials in the form of $Pt/K_2O/Al_2O_3/ZrO_2/TiO_2$ were synthesized with different $K_2O$ loadings. Synthesized materials were structurally characterized *via* XRD and BET in comparison to a conventional Pt/20Ba/Al benchmark NSR/LNT catalyst. Interaction of these catalyst surfaces with $SO_x$ (*i.e.* $SO_2 + O_2$) mixture were monitored spectroscopically using *in-situ* FTIR and TPD. Our findings can be summarized as follows:

- Besides the presence of ordered metallic Pt, Pt/AZT, Pt/2.7K/AZT and Pt/5.4K/AZT materials revealed disordered structures. On the other hand, Pt/10K/AZT exhibited additional diffraction signals corresponding to tetragonal $ZrO_2$ domains. Unlike the AZT-supported materials, conventional Pt/20Ba/Al benchmark catalyst was composed of ordered phases including $\gamma$-$Al_2O_3$ and $BaAl_2O_4$.
- Increase in $K_2O$ loading from 2.7 to 5.4 and 10.0 wt. % monotonically decreases the SSA values from 177 $m^2/g$ to 155 and 125 $m^2/g$, respectively. Apart from the Pt/10K/AZT catalyst, SSA values of the corresponding Pt/K/AZT catalysts are higher than that of the benchmark Pt/20Ba/Al catalyst (134 $m^2/g$).
- Increasing the $K_2O$ loading in the Pt/K/AZT system leads to the growth of the $K_2O$ domain size (*i.e.* sintering), covering of the AZT surface with $K_2O$ and an increase in the bulk-like sulfate functional groups requiring higher temperatures for complete sulfur elimination *via* thermal decomposition or *via* reduction with $H_2$(g).
- Increase in $K_2O$ loading in the Pt/K/AZT formulation increases the $NO_x$ adsorption up to 5.4 wt. % of $K_2O$. However $K_2O$ loadings higher than this value do not have a significant positive influence on $NO_x$ adsorption.
- There is a delicate trade-off between NSC and sulfur adsorption/release/regeneration characteristics. NSC and $SO_x$ tolerance of AZT based NSR/LNT catalysts can be optimized simultaneously by carefully fine-tuning the $K_2O$ loading.
- Among the investigated catalysts, Pt/5.4K/AZT was found to reveal superior sulfur regeneration performance than that of the conventional Pt/20Ba/Al benchmark catalyst along with a comparable NSC (0.165 *vs.* 0.171 mmol/$g_{cat}$, repsectively).

## Acknowledgements

Authors acknowledge the financial support from the Scientific and Technological Research Council of Turkey (TUBITAK) (Project Code: 111M780). Authors also acknowledge Prof. Louise Olsson and Oana Mihai (Chalmers University of Technology) for quantitative flow-mode NSC measurements.

## Appendix A. Supplementary data

Supplementary data associated with this article can be found, in the online version, at http://dx.doi.org/10.1016/j.cattod.2015.12.013.

## References

[1] F. Klingstedt, K. Arve, K. Eränen, D.Y. Murzin, Acc. Chem. Res. 39 (2006) 273–282.
[2] W.S. Epling, L.E. Campbell, A. Yezerets, N.W. Currier, J.E. Parks, Catal. Rev. Eng. 46 (2004) 163–245.
[3] S. Matsumoto, CATTECH 4 (2000) 102–109.
[4] A. Fritz, V. Pitchon, Appl. Catal. B Environ. 13 (1997) 1–25.
[5] Q. Schiermeier, The science behind the Volkswagen emissions scandal, in: Nat. News, 2015.
[6] <http://www.eea.europa.eu/publications/nec-directive-status-report-2014>.
[7] K. Kato, H. Nohira, K. Nakanishi, S. Iguchi, T. Kihara, H. Muraki, Euro Patent application 0,573,672 A1, 1993.
[8] N. Myioshi, S. Matsumoto, K. Katoh, T. Tanaka, K. Harada, N. Takahashi, K. Yokota, M. Sugiura, K. Kasahara, SAE Technical Papers Series No. 950809, 1995.
[9] S. Roy, A. Baiker, Chem. Rev. 109 (2009) 4054–4091.
[10] Z. Say, E.I. Vovk, V.I. Bukhtiyarov, E. Ozensoy, Appl. Catal. B Environ. 142–143 (2013) 89–100.
[11] W.S. Epling, D. Kisinger, C. Everest, Catal. Today 136 (2008) 156–163.
[12] D.H. Kim, Y. Chin, G.G. Muntean, A. Yezeretz, N.W. Currier, W.S. Epling, H. Chen, H. Hess, C.H.F. Peden, Ind. Eng. Chem. Res. 45 (2006) 8815–8821.
[13] S.M. Andonova, G.S. Şentürk, E. Kayhan, E. Ozensoy, J. Phys. Chem. C 113 (2009) 11026.
[14] Z. Say, E.I. Vovk, V.I. Bukhtiyarov, E. Ozensoy, Top. Catal. 56 (2013) 950–957.
[15] T. Szailer, J.H. Kwak, D.H. Kim, J.C. Hanson, C.H.F. Peden, J. Szanyi, J. Catal. 239 (2006) 51–64.
[16] I.S. Pieta, M. García-Diéguez, C. Herrera, M. a. Larrubia, L.J. Alemany, J. Catal. 270 (2010) 256–267.
[17] K.S. Kabin, P. Khanna, R.L. Muncrief, V. Medhekar, M.P. Harold, Catal. Today 114 (2006) 72–85.
[18] S. Morandi, F. Prinetto, G. Ghiotti, L. Castoldi, L. Lietti, P. Forzatti, M. Daturi, V. Blasin-Aubé, Catal. Today 231 (2014) 116–124.
[19] D.H. Kim, K. Mudiyanselage, J. Szányi, H. Zhu, J.H. Kwak, C.H.F. Peden, Catal. Today 184 (2012) 2–7.
[20] M. Takeuchi, S. Matsumoto, Top. Catal. 28 (2004) 151–156.
[21] T.J. Toops, D.B. Smith, W.P. Partridge, Catal. Today 114 (2006) 112–124.
[22] J. Luo, F. Gao, D.H. Kim, C.H.F. Peden, Catal. Today 231 (2014) 164–172.
[23] E. Fridell, H. Persson, L. Olsson, B. Westerberg, A. Amberntsson, M. Skoglundh, Top. Catal. 16/17 (2001) 133.
[24] J. Escobar, J.A. De los Reyes, T. Viveros, Ind. Eng. Chem. Res. 39 (2000) 666.
[25] Z. Say, M. Tohumeken, E. Ozensoy, Catal. Today 231 (2014) 135.

[26] M. Meng, L. Guo, J. He, Y. Lai, Z. Li, X. Li, Catal. Today 175 (2011) 72.
[27] Z.Q. Zou, M. Meng, X.Y. Zhou, X.G. Li, Y.Q. Zha, Catal. Lett. 128 (2009) 475.
[28] N. Takahashi, A. Suda, I. Hachisuka, M. Sugiura, H. Sobukawa, H. Shinjoh, Appl. Catal. B Environ. 72 (2007) 187.
[29] H. Imagawa, T. Tanaka, N. Takahashi, S. Matsunaga, A. Suda, H. Shinjoh, J. Catal. 251 (2007) 315.
[30] H. Imagawa, N. Takahashi, T. Tanaka, S. Matsunaga, H. Shinjoh, Appl. Catal. B Environ. 92 (2009) 23.
[31] Z.Q. Zou, M. Meng, J. He, Mater. Chem. Phys. 124 (2010) 987.
[32] Z. Say, M. Dogac, E.I. Vovk, Y.E. Kalay, C.H. Kim, W. Li, E. Ozensoy, Appl. Catal. B Environ 154–155 (2014) 51.
[33] L.E. Venegas, N.A. Mazzeo, A.L.P. Rojas, Air Qual. Appl., In Tech., 2011, ISBN: 978-953-307-307-1.
[34] D.H. Kim, K. Mudiyanselage, J. Szanyi, J.H. Kwak, H. Zhu, C.H.F. Peden, Appl. Catal. B Environ. 142–143 (2013) 472–478.
[35] M. Kantcheva, E.Z. Ciftlikli, J. Phys. Chem. B 106 (2002) 3941–3949.
[36] C. Chang, J. Catal. 53 (1978) 374–385.
[37] M. Waqif, Solid State Ionics 95 (1997) 163–167.
[38] O. Saur, M. Bensitel, A.B. Mohammed Saad, J.C. Lavalley, C.P. Tripp, B.A. Morrow, J. Catal. 99 (1986) 104–110.
[39] H. Yao, H.K. Stepien, H.S. Gandhi, J. Catal. 67 (1981) 231–236.
[40] G.S. Şentürk, E.I. Vovk, V.I. Zaikovskii, Z. Say, A.M. Soylu, V.I. Bukhtiyarov, E. Ozensoy, Catal.Today 184 (2012) 54–71.
[41] C. Sedlmair, K. Seshan, A. Jentys, J. Lercher, Catal. Today 75 (2002) 413–419.
[42] Y. Liu, M. Meng, X.G. Li, L.H. Guo, Y.Q. Zha, Chem. Eng. Res. Des. 86 (2008) 932–940.
[43] H. Abdulhamid, E. Fridell, J. Dawody, M. Skoglundh, J. Catal. 241 (2006) 200–210.
[44] Z. Say, O. Mihai, M. Tohumeken, L. Olsson, E. Ozensoy, in preperation.